ACS OMEGA

http://pubs.acs.org/journal/acsodf

Article

Core–Shell Polydopamine/Cu Nanometer Rods Efficiently Deactivate Microbes by Mimicking Chloride-Activated Peroxidases

Lian-Jiao Zhou, Yu-Ying Wang, Shu-Lan Li, Ling Cao, Feng-Lei Jiang, Thomas Maskow,* and Yi Liu*

Cite This: *ACS Omega* 2022, 7, 29984–29994

Read Online

ACCESS | Metrics & More | Article Recommendations | Supporting Information

ABSTRACT: Cu-modified nanoparticles have been designed to mimic peroxidase, and their potent antibacterial and anti-biofilm abilities have been widely investigated. In this study, novel core–shell polydopamine (PDA)/$Cu_4(OH)_6SO_4$ crystal (PDA/Cu) nanometer rods were prepared. The PDA/Cu nanometer rods show similar kinetic behaviors to chloride-activated peroxidases, exhibit excellent photothermal properties, and are sensitive to the concentrations of pH values and the substrate (i.e., H_2O_2). PDA/Cu nanometer rods could adhere to the bacteria and catalyze hydrogen peroxide (H_2O_2) to generate more reactive hydroxy radicals (•OH) against *Staphylococcus aureus* and *Escherichia coli*, Furthermore, PDA/Cu nanometer rods show enhanced catalytic and photothermal synergistic antibacterial activity. This work provides a simple, inexpensive, and effective strategy for antibacterial applications.

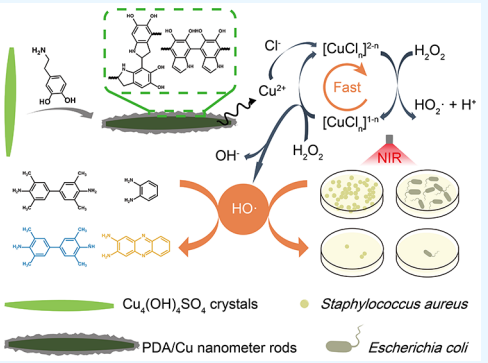

INTRODUCTION

Antibiotic-resistant bacterial infections are posing a serious threat to public health. Bacteriostatic antibiotics act on bacteria by targeting and disrupting their basic survival (bactericidal) and multiplication (bacteriostatic) processes.[1] However, microorganisms rapidly evolve antibiotic resistance through gene mutation and horizontal gene transfer, changes in antibiotic targets, or modification of the antibiotic agents.[1,2] Therefore, Cu-modified nanoparticles with efficient antibacterial properties were developed, and they use multiple mechanisms simultaneously to kill and/or inhibit the growth of microorganisms, overcoming microbial resistance mechanisms.[3−5]

Cu-modified nanoparticles were recently reported to exhibit peroxidase-like activity and consequently could conceivably be used as antibacterial materials.[6] Nanoparticles working as artificial enzymes keep their catalytic activity in extreme pH and temperature conditions[7] and have higher stability and lower price and are easier to be stored compared with natural enzymes.[8] The peroxidase-like catalytic mechanism of Cu-based nanomaterials is generally summarized as a Fenton-like reaction.[9] Briefly, Cu^{2+} ions participate in catalyzing the conversion of hydrogen peroxide (H_2O_2) to hydroxyl radicals (•OH).[10] •OH is much more effective against microorganisms than H_2O_2,[11,12] since H_2O_2 is less reactive and can be detoxified by endogenous antioxidants.[13] Accelerated rates of •OH production correlate remarkably with antibacterial activities.[14]

In addition to Cu or Cu compound nanomaterials being used as nanozymes, it was also reported that the adhesion of Cu^{2+} on organic nanomaterials significantly improved the enzyme-like catalytic activity of nanozymes and enhanced synergistic antibacterial activity.[6,15,16] Polydopamine (PDA) has been recently widely used in antibacterial composite materials, benefiting from its advantages of easy synthesis, good biocompatibility, strong adhesion, excellent photothermal properties, and unique antibacterial ability.[17] It was reported that PDA was used to modify the surface of nanozyme to improve their antibacterial effect and ability to target the bacteria membrane.[17,18] Moreover, the photothermal effect of PDA provided the composite nanozymes with additional photothermal therapy and near-infrared (NIR)-enhanced catalytic activity to augment their antibacterial activity.[19,20]

In this study, we developed a simple method to prepare core–shell PDA/$Cu_4(OH)_6SO_4$ crystal (PDA/Cu) nanometer rods. PDA/Cu nanometer rods showed Cl^--accelerated peroxidase-like activity. In phosphate-buffered saline (PBS) buffer containing sufficient Cl^-, the antibacterial activity of PDA/Cu and H_2O_2 against *Staphylococcus aureus* and *Escherichia coli* was much higher than that of H_2O_2 alone. Furthermore, PDA/Cu nanometer rods have an excellent photothermal property compared with non-PDA $Cu_4(OH)_6SO_4$ crystals, which endowed them with enhanced catalytic and photothermal synergistic antibacterial activity.

Received: May 13, 2022
Accepted: August 3, 2022
Published: August 17, 2022

https://doi.org/10.1021/acsomega.2c02986
ACS Omega 2022, 7, 29984–29994

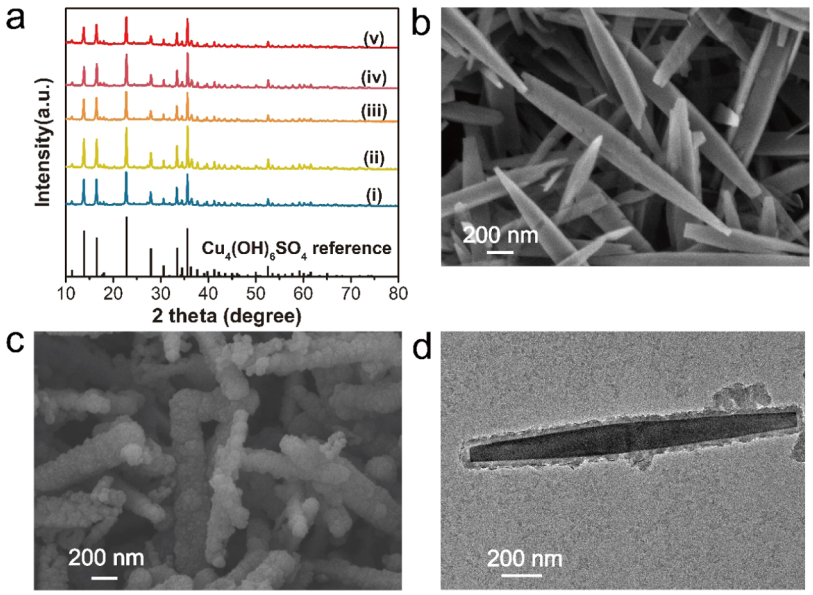

Figure 1. Characterization of the chemical structure of PDA/Cu nanometer rods. (a) XRD patterns of (i) the obtained $Cu_4(OH)_6SO_4$ crystals and PDA/Cu nanometer rods prepared for (ii) 0.5 h, (iii) 1 h, (iv) 3 h, and (v) 9 h. $Cu_4(OH)_6SO_4$ (brochantite) reference is presented for comparison. (b) SEM images of $Cu_4(OH)_6SO_4$ crystals. (c) SEM and (d) TEM images of PDA/Cu nanometer rods obtained after 9 h of reaction time.

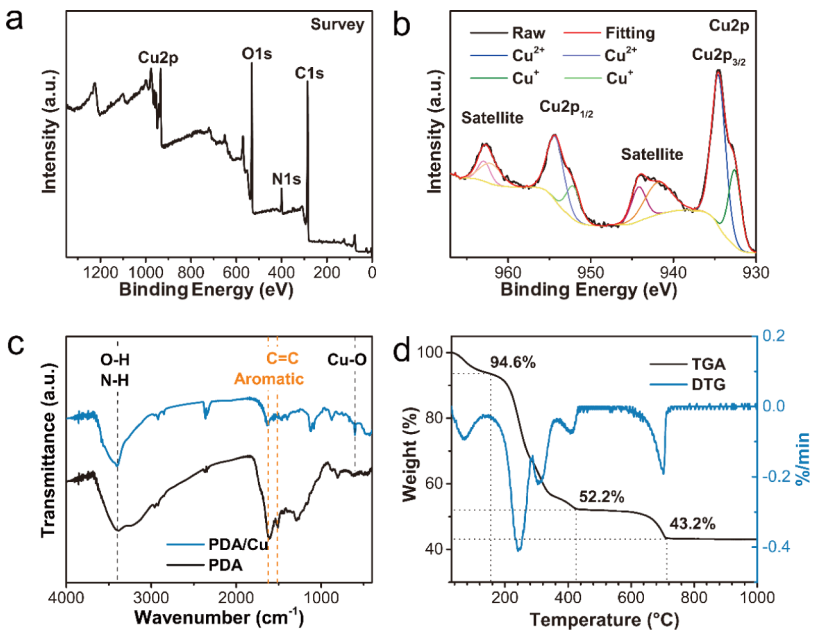

Figure 2. Characterization of the chemical structure of PDA/Cu nanometer rods. (a) XPS spectrum. (b) High-resolution XPS spectrum of Cu 2p. (c) Fourier transform infrared (FT-IR) of self-polymerized PDA and PDA/Cu nanometer rods. (d) Thermogravimetric analysis (TGA)/derivative thermogravimetry (DTG) curves of PDA/Cu nanometer rods.

RESULTS AND DISCUSSION

Synthesis and Characterization of PDA/Cu Nanometer Rods. .PDA/Cu nanometer rods were synthesized via a simple method. The green suspension of $Cu_4(OH)_6SO_4$ crystals (brochantite) was prepared in the aqueous mixture of $CuSO_4{\cdot}5H_2O$ and NaAc (pH = 5),[21] in a molar proportion of Cu^{2+}/Ac^{-} = 1/6. The excessive addition of Ac^{-} was to keep the aqueous solution in slightly acidic conditions to fit with the narrow stability field of brochantite.[22] Subsequently, DA·HCl was added, and the green suspension turned brown immediately, reflecting the formation of PDA. The X-ray diffraction (XRD) pattern of the obtained $Cu_4(OH)_6SO_4$ crystals is shown in Figure 1a. The characteristic peaks of the obtained crystals are consistent with the reference brochantite, indicating that the main component of the green suspension is $Cu_4(OH)_6SO_4$ crystals. Moreover, it was concluded from the slight difference between the XRD patterns of the $Cu_4(OH)_6SO_4$ crystals and PDA/Cu nanometer rods that the coating with PDA did not disrupt the structure of the $Cu_4(OH)_6SO_4$ crystals greatly. As shown in the transmission electron microscopy (TEM) images and scanning electron microscopy (SEM) images (Figure 1b–d), the core–shell PDA/Cu nanometer rods had a length of 1–2 μm and a maximum width of 200 nm, with the thickness of the PDA

https://doi.org/10.1021/acsomega.2c02986
ACS Omega 2022, 7, 29984–29994

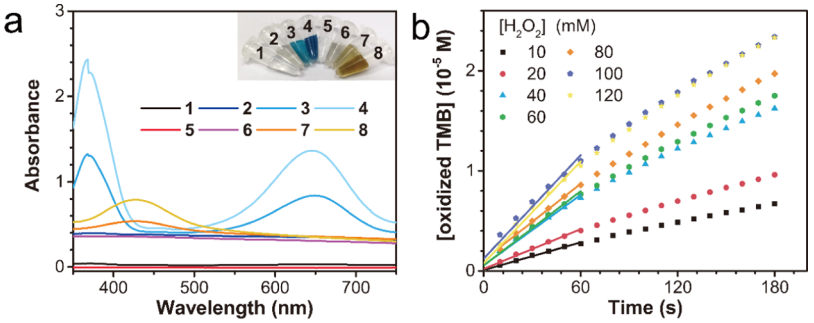

Figure 3. (a) UV−vis absorption spectra of colorimetric substrates: (1) TMB + NH_4Cl + H_2O_2, (2) TMB + NH_4Cl + PDA/Cu, (3) TMB + H_2O_2 + PDA/Cu, (4) TMB + NH_4Cl + H_2O_2 + PDA/Cu, (5) OPD + NH_4Cl + H_2O_2, (6) OPD + NH_4Cl + PDA/Cu, (7) OPD + H_2O_2 + PDA/Cu, (8) OPD + NH_4Cl + H_2O_2 + PDA/Cu (TMB: 0.5 mM, OPD: 0.5 mM, NH_4Cl: 100 mM, H_2O_2: 100 mM, PDA/Cu: 50 μg mL^{-1}, solution: 0.1 M 2-(*N*-morpholino)ethanesulfonic acid (MES) buffer, pH 5.5). (b) Kinetics of the TMB oxidation as a function of the H_2O_2 concentration. The lines show the linear data interpolation of the first 60 s.

coating of about 30 nm. The dynamic light scattering (DLS) study suggested that the PDA/Cu nanometer rods had a hydrodynamic diameter of 1237 ± 20 nm. The formation process of PDA/Cu nanometer rods was additionally monitored by SEM. According to the SEM images of PDA/Cu nanometer rods shown in Figure S1 in the Supporting Information (SI), the coating of $Cu_4(OH)_6SO_4$ crystals with PDA increased the roughness of the surface and led to the inconsistent morphology of PDA/Cu nanometer rods. We proposed that there were three major factors that led to this: (1) The $Cu_4(OH)_6SO_4$ crystals cores had different thicknesses and lengths. (2) The self-polymerized PDA nanoparticles catalyzed by the free Cu^{2+} in the reaction solution are mixed with PDA/Cu nanometer rods.[23] (3) Because of the Cu^{2+} chelating capability of dopamine and its derivates, PDA promoted the etching of $Cu_4(OH)_6SO_4$ crystals cores, resulting in either pure PDA capsules or ill-defined structures.[24]

The elemental composition of PDA/Cu nanometer rods was characterized by X-ray photoelectron spectroscopy (XPS). Four main peak groups of C 1s, N 1s, O 1s, and Cu 2p were observed in the PDA/Cu nanometer rod sample (Figure 2a), which was ascribed to the $Cu_4(OH)_6SO_4$ crystals and the PDA layer formed on its surface. The high-resolution XPS spectrum of Cu 2p is shown in Figure 2b. The binding energies of Cu^{2+} 2p (3/2) and Cu^{2+} 2p (1/2) were observed at 934.6 and 954.4 eV, with the Cu^+ 2p (3/2) and Cu^+ 2p (1/2) at 932.6 and 952.2 eV, respectively. The satellite peaks in the spectra confirmed that PDA/Cu nanometer rods contain both Cu^{2+} and Cu^+ ions. The reduction of Cu^{2+} to Cu^+ could be caused by the oxidative polymerization process. Cu^{2+} has been reported as an oxidizing agent to speed up the polymerization process of DA. In this process, DA was catalytically oxidized to the *o*-quinone of DA with the generation of $^{\bullet}O_2^-$ and Cu^+, and then Cu^+ was reoxidized by O_2 and $^{\bullet}O_2^-$ to form Cu^{2+}.[23,25] Although Cu^{2+} alone was a weak oxidant under acidic conditions, the Cl^- from DA·HCl facilitated the reaction.[23,26] This is because Cl^- increases the positive redox potential of Cu^{2+}/Cu^+ due to the formation of strong Cu^+-Cl^- complexes.[33] The high-resolution XPS spectrum of N 1s (Figure S2a in the SI) was decomposed into three peaks corresponding to the nitrogen environments of RNH_2 (401.1 eV), R_2NH (399.8 eV), and Aryl-NH (398.5 eV). The O 1s spectrum (Figure S2b in the SI) was separated into two peaks with binding energies of 532.6 and 531.3 eV, which were assigned to C−O and C═O, respectively. The three peaks of C 1s (Figure S2c in the SI) at 284.5, 285.4, and 287.6 eV were assigned to C═O, C−O/C−N, and C−C/C−H of PDA.

FT-IR test (Figure 2c) was done to reveal the chemical structure of the self-polymerized PDA and PDA/Cu nanometer rods. PDA/Cu nanometer rods had an absorption peak at 603 cm^{-1}, which is the characteristic of Cu−O vibration. In the spectra of both self-polymerized PDA and PDA/Cu nanometer rods, the peaks located at the wavenumber of 3404 cm^{-1} were related to the N−H stretching vibrations and catechol O−H stretching vibrations. The peaks at 1640−1510 cm^{-1} were caused by the benzene skeleton vibrations. The identified hydroxyl, amine groups, and aromatic structure in the two spectra were evidence of the formation of PDA on the surface of $Cu_4(OH)_6SO_4$ crystals. The above characterizations demonstrated the successful preparation of core−shell PDA/Cu nanometer rods.

The content of the Cu element in PDA/Cu nanometer rods was measured by TGA. The first weight drop in the TGA curve between 30 and 120 °C (Figure 2d) was presumably due to the evaporation of the surface-adsorbed water.[27,28] The significant change in weight from 170 to 430 °C was ascribed to the thermal degradation of PDA coating, and the structural water came from the OH^- groups of $Cu_4(OH)_6SO_4$ crystals. The decomposition of copper sulfate ($CuSO_4$) happened between 430 and 710 °C, which was also observed in the TGA and DTG curves of $Cu_4(OH)_6SO_4$ crystals (see Figure S3). There was almost no weight loss between 710 and 1000 °C, indicating that the complete decomposition was achieved and the decomposition product was CuO,[29] with a mass percentage of 43.2%.

Peroxidase-Like Activity of PDA/Cu Nanometer Rods and Kinetic Studies. The peroxidase-like catalytic activity of PDA/Cu nanometer rods was photometrically quantified. For that purpose, the color changes of 3,3′,5,5′-tetramethylbenzidine (TMB) ($\varepsilon_{652\ nm}$ = 39 000 M^{-1} cm^{-1}) and *o*-phenylenediamine (OPD) ($\varepsilon_{417\ nm}$ = 16 700 M^{-1} cm^{-1}) oxidized with H_2O_2 were monitored in presence of PDA/Cu nanometer rods.

Figure 3a shows the UV−vis absorption spectra of the oxidation products of the mixtures of TMB, PDA/Cu nanometer rods, and H_2O_2 after a 1 min of reaction time at 25 °C. The appearance of two absorption peaks at 370 and 652 nm indicated that colorless TMB was oxidized to its colored products. However, the absence of the absorption peaks in the sample without PDA/Cu nanometer rods or H_2O_2 indicated the catalytic activity of the PDA/Cu nanometer rods and the

https://doi.org/10.1021/acsomega.2c02986
ACS Omega 2022, 7, 29984−29994

requirement of oxidative power. Moreover, when Cl^- was added to the mixture containing TMB, PDA/Cu nanometer rods, and H_2O_2, more oxidized TMB was obtained, indicated by the higher absorption peaks at 370 and 652 nm. The same results were obtained from the absorption spectra of OPD. These results suggested that PDA/Cu nanometer rods had a peroxidase-like catalytic ability, and the addition of Cl^- accelerated this process. The Cl^--accelerated mechanism could be explained by the fact that the coordination of Cl^- stabilized Cu^+ more than Cu^{2+}. This led to an enhanced formation of Cu^+ from Cu^{2+}, which was the rate-determining step of the Cu^{2+}-catalyzed decomposition of H_2O_2.[10,30]

The absorbance at 652 nm was considered as a measure of the progress of TMB oxidation. The initial stage was linearly approximated and the slope was considered as the initial reaction rate (shown in Figure 3b). The plots of the initial reaction rates as a function of the concentrations of TMB and H_2O_2 clearly followed a Michaelis−Menten kinetic (see Figure S4 in the SI). The kinetic parameters of K_m and V_{max} were obtained from the nonlinear parameter fitting of the Michaelis−Menten equation to the experimental data. Table 1 compared the kinetic parameters of PDA/Cu nanometer rods with horseradish peroxidase (HRP) and other peroxidase mimics. The results show that PDA nanometer rods have higher V_{max} for both H_2O_2 and TMB than other nanozymes.

Table 1. Kinetic Parameters for the Peroxidase-Like Activity of PDA/Cu Nanometer Rods, Other Mimics, and HRP

	K_m (mM)		V_{max} (10^{-8} M s^{-1})	
	TMB	H_2O_2	TMB	H_2O_2
PDA/Cu nanometer rods	2.66	39.93	70.3	15.8
Fe_3O_4[31]	0.098	154	3.44	9.78
MOF-808[32]	0.0796	1.06	3.12	1.39
Cu-CDs[33]	0.042	67.4	8.26	1.96
HRP[34]	0.172	10.9	41.8	58.5

Temperature, pH, and Solution-Dependent Peroxidase-Like Activity. Selected factors that may affect the peroxidase-like catalytic activity of PDA/Cu nanometer rods were explored. For that purpose, the initial rate versus Cl^- concentrations were analyzed (Figure 4a). A linear Cl^--accelerating effect on the peroxidase-like activity of PDA/Cu nanometer rods in the Cl^- concentrations in the range from 10 to 125 mM was observed. Figure 4b shows the catalytic activity as a function of pH in the range of 3.0−8.0, with an optimum between 4.5 and 5.0.

To study the relationship between catalytic activity and temperature, we chose OPD as the chromogenic substrate instead of TMB, which had two oxidation products at 60 °C with different UV−vis absorption spectra (see Figure S5 and Scheme S1a in the SI). In contrast, OPD provided a color response that maintained its maximum absorption peak without unacceptable changes at elevated temperatures (Figure 5a and Scheme S1b). PDA/Cu nanometer rods showed a higher initial rate at higher temperatures between 25 and 65 °C, with a good linear relation between the natural logarithm of the kinetic constant and the reciprocal temperature (Figure 5b). The data fitted well with the Arrhenius equation, and the calculated activation energy of the reaction was 78.48 ± 2.86 kJ mol^{-1} (Figure 5c). The final absorbance of H_2O_2 + OPD was much lower than that of the H_2O_2 + OPD + PDA/Cu system or the H_2O_2 + OPD + PDA/Cu + NH_4Cl system (see Figure S6 in the SI), indicating the lower catalytic activity of the H_2O_2 + OPD system. Compared with the H_2O_2 + OPD + PDA/Cu system (E_a = 84.49 ± 4.24 kJ mol^{-1}), the OPD + NH_4Cl + H_2O_2 + PDA/Cu system (E_a = 78.48 ± 2.86 kJ mol^{-1}) had faster kinetics at the same temperature, and the reaction mechanism required lower activation energy.

The above-mentioned results indicated that PDA/Cu nanometer rods had higher stability at extreme temperature conditions and were easier to be stored compared with natural enzymes.[35] Additionally, PDA/Cu nanometer rods showed higher V_{max} than other nanozymes and had higher catalytic activity at higher temperatures, while some other nanozymes have optimum activity at a temperature of around 40 °C[31,36] or showed stable catalytic activity in a wide temperature range.[7]

The peroxidase-like activity of PDA/Cu nanometer rods depended on the applied buffer solution (Figure 5d and Table S1 in the SI). The catalytic activity of PDA/Cu nanometer rods in the MES buffer was higher than that in the BR buffer at the same pH. This was because Ac^- was tightly adsorbed on Cu^{2+} and resulted in a negatively charged surface. In contrast, 2-(*N*-morpholino)ethanesulfonic acid (MES) hardly was bound to Cu^{2+} at pH < 7.[37] The catalytic activity of the PDA/Cu nanometer rods in the PBS buffer (pH 5.0) reached a particularly high level due to the high concentration of Cl^- in the PBS buffer.

Peroxidase-Like Catalytic Antimicrobial Activity. Two samples of potentially pathogenic bacteria (the Gram-positive bacteria *S. aureus* and the Gram-negative bacteria *E. coli*) were chosen to evaluate the antibacterial activity of the PDA/Cu + H_2O_2 + Cl^- system. The experiments were performed in the PBS buffer at pH 5.0 because PDA/Cu showed the highest catalytic activity at pH 5.0 (Figure 4b), and the high

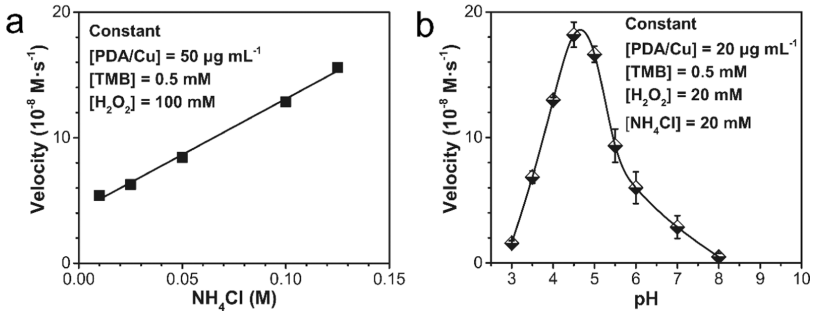

Figure 4. (a) Colorimetric assay based on Cl^--accelerated peroxidase-like activity of PDA/Cu nanometer rods. (b) pH-dependent peroxidase-like activity of PDA/Cu nanometer rods carried out in Britton−Robison (BR) buffer (25 °C) (n = 3 for each data point).

https://doi.org/10.1021/acsomega.2c02986
ACS Omega 2022, 7, 29984−29994

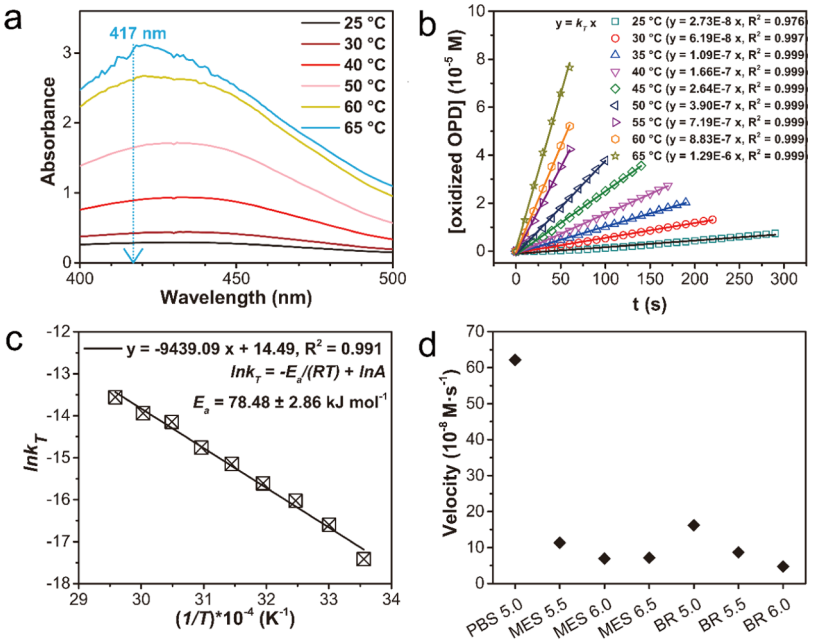

Figure 5. (a) UV−vis absorption spectra of oxidized OPD in the temperature range of 25−65 °C (OPD: 0.5 mM, H_2O_2: 20 mM, NH_4Cl: 20 mM; PDA/Cu nanometer rods: 10 μg mL^{-1}, incubation for 5 min). (b) Plots of the concentration of oxidized OPD versus time. The slope is the rate constant. (c) Plots of ln k_T versus 1/T. The slope is the activation energy. (d) Initial reaction rates in different pH buffers.

concentration of Cl^- in the PBS buffer greatly increased the Cl^--accelerated peroxidase-like activity (Figure 5d). The PBS buffers of pH 5.0 and 7.4 had no significant influence on the survival of both sample bacterial strains, as demonstrated by colony-forming units (CFUs) after incubation for 1 h at 37 °C (see Figure S7 in the SI).

Agar plates were used to determine the survival of bacteria after incubation with PDA/Cu nanometer rods and H_2O_2 for 1 h. As shown in the photographs of agar plates (Figure 6a), both the growth of *S. aureus* and *E. coli* were suppressed by PDA/Cu nanometer rods in combination with H_2O_2, whereas both agents alone have no such significant effect.

SEM images were taken to visualize the changes in bacterial membrane and structure after exposure to different treatments (Figure 6b). After incubation with PDA/Cu nanometer rods, both *S. aureus* and *E. coli* had a smooth membrane and an intact cell structure consistent with the control, indicating that PDA/Cu nanometer rods did not cause fatal damage to the bacteria. In contrast, partial deformation and shrinkage of bacteria appeared after incubation with H_2O_2. Furthermore, in the group of PDA/Cu nanometer rods with H_2O_2, the bacteria showed major damage and lost their intact spherical-like or rod-like shape. The adhesion of bacteria to PDA/Cu nanometer rods was also observed, which would facilitate the rapid and precise attack of $^{\bullet}OH$ from the surface of PDA/Cu nanometer rods to the cell membrane.

A plate-counting method was applied for quantifying the influence of the different agents on the survival of the bacteria. PDA/Cu nanometer rods in the concentration range of 0−20 μg mL^{-1} alone did not show high antibacterial activity (Figure 6c,d). After the addition of H_2O_2, the number of viable bacteria decreased significantly with the increase in the PDA/Cu nanometer rod concentrations. The survival rates of both *S. aureus* and *E. coli* were less than 0.01% when the concentration of PDA/Cu nanometer rods was higher than 10 μg mL^{-1}. H_2O_2 was able to kill 99.9% of *S. aureus* and *E. coli* at concentrations of 100 and 10 mM, respectively (Figure 6e,f). Compared with *E. coli*, *S. aureus* required higher concentrations of H_2O_2 to effectively inactivate bacteria. The remarkable H_2O_2 resistance of *S. aureus* was known to be caused by antioxidant enzymes (superoxide dismutases, catalases, and peroxiredoxins), which participated in the detoxification of $^{\bullet}O_2^-$ and H_2O_2 but not of $^{\bullet}OH$.[13,38] The PDA/Cu nanometer rods catalyzed the conversion of H_2O_2 to the potent antibacterial agent $^{\bullet}OH$. Approximately 20 mM H_2O_2 was required for *S. aureus* and 5 mM for *E. coli* to achieve a similar antibacterial activity.

To clarify whether the PDA/Cu nanometer rods or the released Cu^{2+} played a major role in the antibacterial process, the release of Cu^{2+} in the PBS buffer (pH 5.0) was quantified by photometric analysis with the chromogenic probe dicyclohexanoneoxaly dihydrazone using the absorbance at 540 nm (Figure 7a).[33,39] According to TGA and DTG results, the molar concentration of Cu in 1 mg mL^{-1} PDA/Cu nanometer rods was 5.4 mM (Figure 2d). In contrast, the absorbance of filtrates of PDA/Cu nanometer rods after different incubation times was much lower than that of 0.6 mM Cu^{2+}, indicating that very little Cu^{2+} was released into the solution.

The antibacterial activity of recollected PDA/Cu nanometer rods from the PBS buffer (pH 5.0) was tested. The nearly identical CFU counts results between PDA/Cu nanometer rods and the recollected ones indicated that the antimicrobial activity mainly remained. In conclusion, the recollected PDA/Cu nanometer rods, after being dispersed in the PBS buffer (pH 5.0), had equal enzyme mimicry-assisted antimicrobial activity to kill 99.9% of *S. aureus* and *E. coli* (Figure 7b). These results demonstrated that PDA/Cu nanometer rods adhered to the bacteria and generated efficiently $^{\bullet}OH$ in the presence of H_2O_2, causing rapid damage to the bacteria.

Photothermal and Catalytic Synergistic Antibacterial Therapy. Numerous studies have reported PDA and PDA composites as photothermal materials with a strong ability to

https://doi.org/10.1021/acsomega.2c02986
ACS Omega 2022, 7, 29984−29994

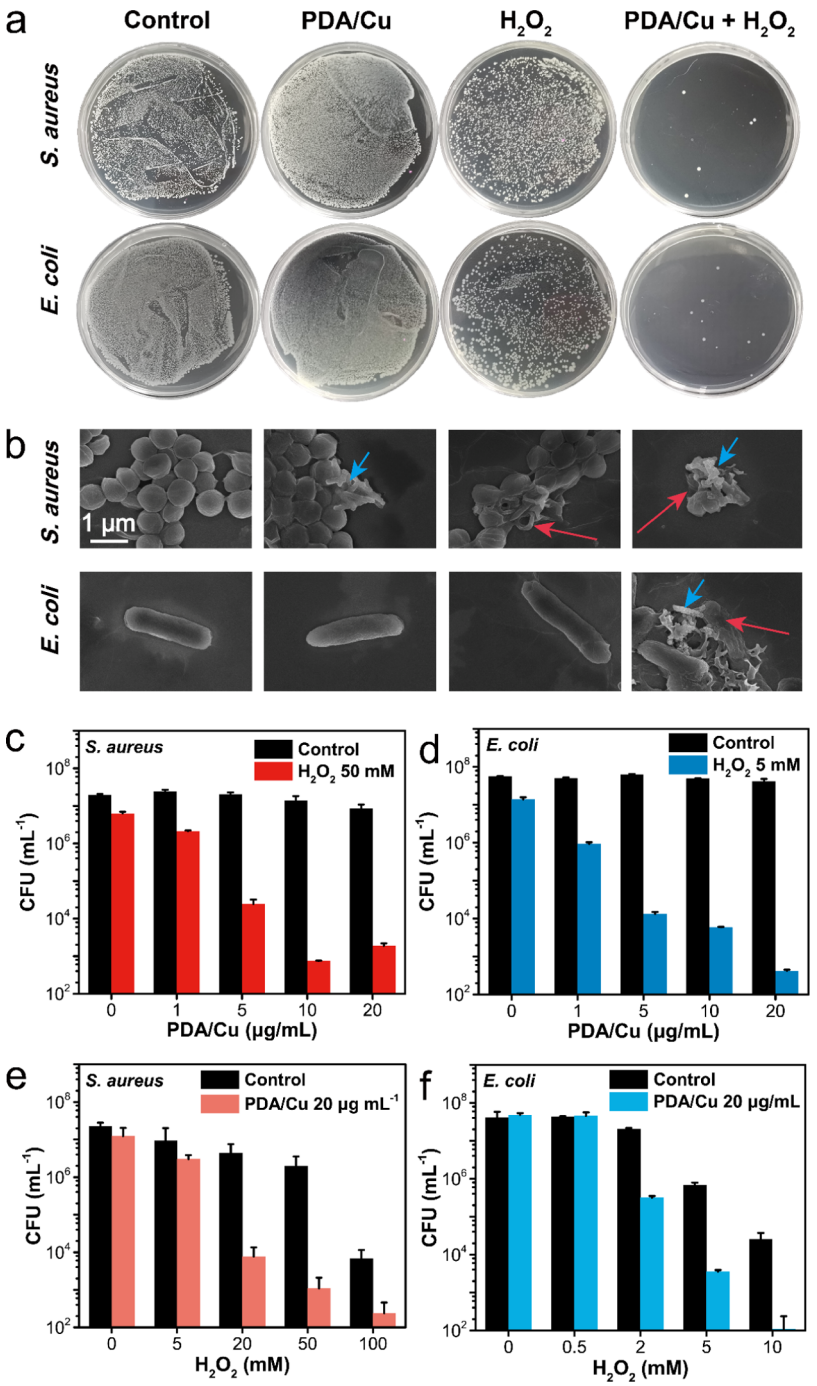

Figure 6. (a) Typical photographs of the agar plates of *S. aureus* and *E. coli* (both about 5×10^7 CFU mL^{-1}) after incubation with different agents with the following concentrations (PDA/Cu nanometer rods: 20 μg mL^{-1}, H_2O_2: 50 mM (*S. aureus*) or 5 mM (*E. coli*)). In the control experiments, nothing was added. (b) SEM images of *S. aureus* and *E. coli* (both about 1×10^9 CFU mL^{-1}) after incubation with different agents with the following concentrations (PDA/Cu nanometer rods: 40 μg mL^{-1}, H_2O_2: 200 mM (*S. aureus*) or 50 mM (*E. coli*)), PDA/Cu nanometer rods were marked with blue arrows and cell membrane damage was marked with red arrows. Colony-forming units (CFUs) of *S. aureus* (c) and *E. coli* (d) after incubation with different concentrations of PDA/Cu nanometer rods with and without H_2O_2 (50 and 5 mM, respectively). CFUs of *S. aureus* (e) and *E. coli* (f) after incubation with different concentrations of H_2O_2 with or without PDA/Cu nanometer rods (20 μg mL^{-1}).

absorb near-infrared light and convert light energy to heat.[40] It was coordinated with the properties of PDA/Cu nanometer rods that exhibited higher catalytic activity at higher temperatures (Figure 5c). Therefore, we studied the photothermal properties of PDA/Cu nanometer rods. The PDA/Cu nanometer rods displayed a monotonously changing UV−vis absorption spectrum (Figure 8a), with a peak at 270 nm and smaller shoulders at 370, 460, and 660 nm, the shoulders could be related to the partially oxidated state of the metal-oxidized polydopamine.[23,41] Moreover, compared to the $Cu_4SO_4(OH)_6$ crystals (Figure S8a in the SI), PDA/Cu nanometer rods displayed a remarkably higher NIR absorption, which was contributed by the PDA layer and was favorable for photothermal therapy. With the NIR irradiation at 808 nm (0.5 W cm^{-2}), the temperature of PDA/Cu nanometer rods increased over time (Figure 8b). The changes in temperatures

https://doi.org/10.1021/acsomega.2c02986
ACS Omega 2022, 7, 29984−29994

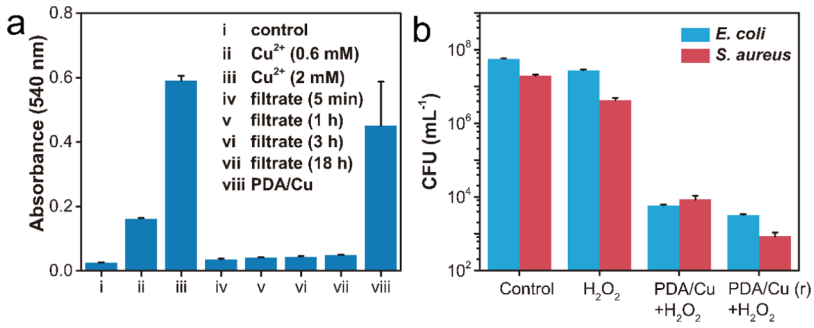

Figure 7. (a) Release of Cu^{2+} from PDA/Cu nanometer rods. (b) CFU of *S. aureus* and *E. coli* after incubation with H_2O_2 (50 and 5 mM, respectively), PDA/Cu nanometer rods (20 μg mL^{-1}) + H_2O_2, and the recollected PDA/Cu nanometer rods (PDA/Cu (*r*), 20 μg mL^{-1}) + H_2O_2.

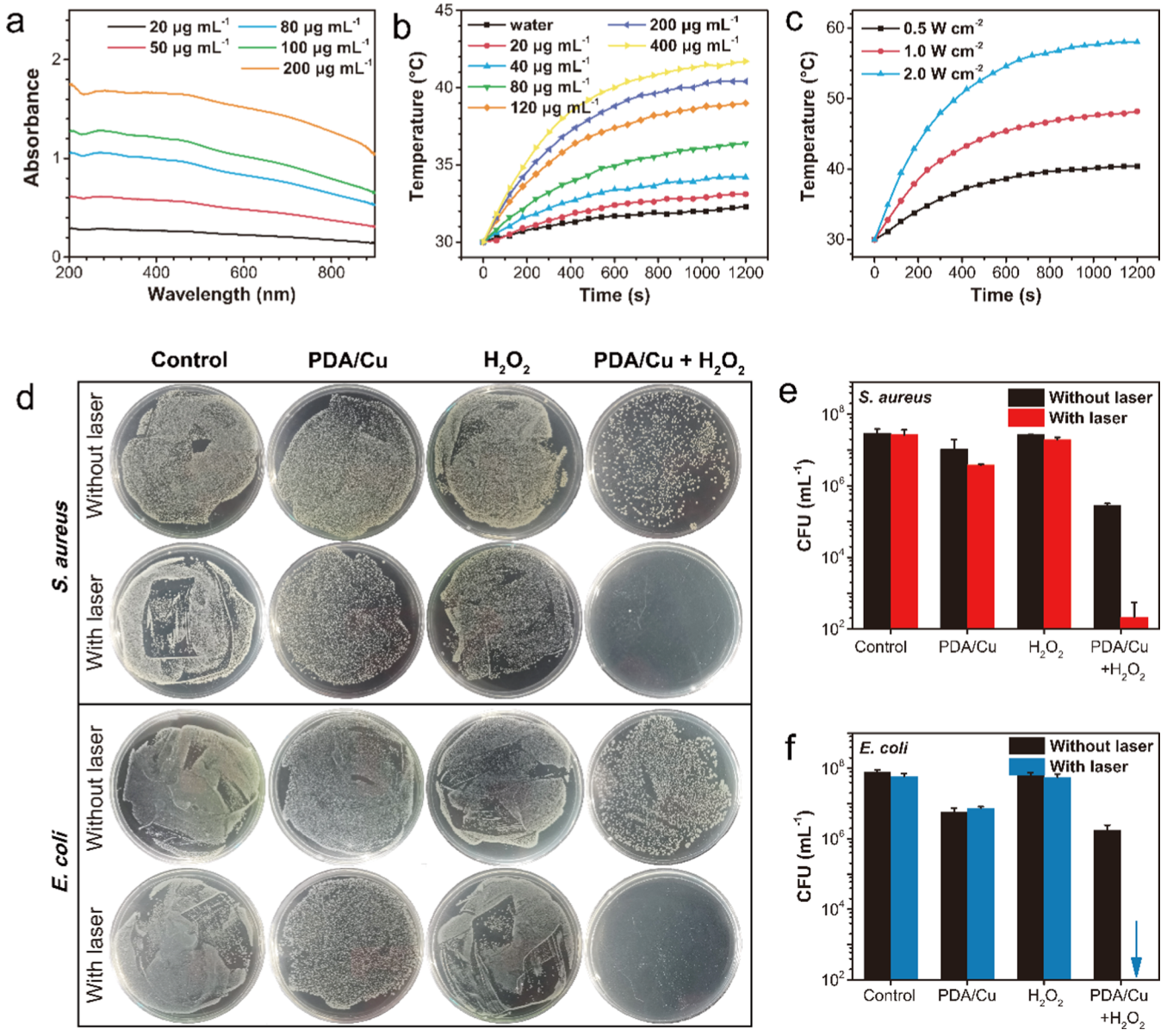

Figure 8. (a) UV−vis absorption spectra of PDA/Cu nanometer rods with different concentrations. (b) Photothermal effects of PDA/Cu nanometer rods at different concentrations at 2.0 W cm^{-2} (λ = 808 nm) and (c) under different power densities (200 μg mL^{-1}). Photothermal and catalytic synergistic antibacterial properties: (d) typical photographs of *S. aureus* and *E. coli* agar plates. (e, f) CFU of *S. aureus* and *E. coli* (PDA/Cu nanometer rods: 80 μg mL^{-1}, H_2O_2: 20 mM (*S. aureus*) or 5 mM (*E. coli*), irradiation laser: 808 nm, 40 mW cm^{-2}; all groups were incubated for 20 min).

https://doi.org/10.1021/acsomega.2c02986
ACS Omega 2022, 7, 29984−29994

were dependent on the concentrations of PDA/Cu nanometer rods and the power densities (Figure 8b,c). As shown in Figure S8b,c in the SI, the photothermal conversion efficiency (η) of PDA/Cu nanometer rods was 22.39%, which was greatly higher than that of pure $Cu_4(OH)_6SO_4$ crystals (0.14%).

With temperature-dependent peroxidase-like activity and photothermal performance, the photothermal and catalytic synergistic antibacterial activity of PDA/Cu nanometer rods were investigated. The synergistic antibacterial effect of PDA/Cu nanometer rods against bacteria was clearly observed through the typical photographs of the agar plate incubated with *S. aureus* and *E. coli* (Figure 8d). The results indicated that Figure 6PDA/Cu nanometer rods had enhanced nanozyme-photothermal antibacterial activity, efficiently killing bacteria in 20 min (Figure 8e,f).

CONCLUSIONS

In summary, core−shell PDA/Cu nanometer rods were obtained with the $Cu_4(OH)_6SO_4$ crystal core and PDA coating. The formation of $Cu_4(OH)_6SO_4$ crystals and polymerization of DA was carried out in a weakly acidic aqueous solution, accompanied by the reduction of Cu^{2+} ions. The obtained PDA/Cu nanometer rods acted similar to the Cl^--activated peroxidase with the activation energy of 78.48 ± 2.86 kJ mol^{-1}. PDA/Cu nanometer rods showed tunable peroxidase-like catalytic activity, which could be easily enhanced by increasing the temperature as well as increasing the concentration of Cl^-. Further studies demonstrated that PDA/Cu nanometer rods showed enhanced catalytic and photothermal synergistic antibacterial activity. In addition, PDA/Cu nanometer rods potentially functionalize material surfaces for efficient synergistic antibacterial properties due to the unique ability of the PDA coating to deposit on almost all inorganic and organic substrates.

EXPERIMENTAL SECTION

Materials. $CuSO_4·5H_2O$ (99.0%), *o*-phenylenediamine (OPD, 98.5%), H_2O_2 (30.0%), ammonium chloride (NH_4Cl, 99.5%), sodium phosphate dibasic dodecahydrate ($Na_2HPO_4·12H_2O$, 99.0%), potassium phosphate monobasic (KH_2PO_4, 99.5%), sodium chloride (NaCl, 99.5%), potassium chloride (KCl, 99.5%), acetic acid (HAc, 99.5%), phosphoric acid (H_3PO_4, 85%), boric acid (H_3BO_3, 99.5%), sodium hydroxide (NaOH, 96%), and hydrochloric acid (HCl, 36.0−38.0%) were purchased from Sinopharm Chemical Reagent Co., Ltd., Shanghai. Sodium acetate (NaAc, 99%) was bought from Acros Organics, Belgium. DA·HCl (98%) and 3,3′,5,5′-tetramethylbenzidine (TMB) (98%) were purchased from Aladdin Industrial Inc., Shanghai. 2-(*N*-Morpholino)-ethanesulfonic acid (MES, 99%) was purchased from Macklin Biochemical Co. Ltd. Shanghai. All these chemicals were used directly without any further purification. All aqueous solutions were prepared in ultrapure water with a resistivity of 18.2 MΩ cm^{-1} (Millipore Simplicity). The composition and the pH range of MES, Britton−Robison (BR), and phosphate-buffered saline (PBS) buffer solutions are listed in Table S1 in the SI.

Characterization. The morphologies of $Cu_4(OH)_6SO_4$ crystals and PDA/Cu nanometer rods were characterized by transmission electron microscopy (TEM) on JEM-2100 Plus (JOEL, Japan) and scanning electron microscopy (SEM) on Zeiss Merlin Compact (Oxford, U.K.). The dynamic light scattering (DLS) measurements were performed on Malvern Instruments Zetasizer Nano (Malvern Instruments, U.K.) at 25 °C. TGA and DTG analysis of PDA/Cu nanometer rods were performed on a Mettler-Toledo TGA2 (Mettler-Toledo, Switzerland) instrument by heating 10 mg of PDA/Cu nanometer rods at a rate of 10 °C min^{-1} from 30 to 1000 °C in a flow of air. The X-ray diffraction (XRD) measurements were recorded on an XPert Pro X-ray diffractometer (Panaco, the Netherlands). The Fourier transform infrared (FT-IR) was conducted on a Nicolet IS10 Fourier transform infrared spectroscope (Thermo Fisher Scientific). The X-ray photoelectron spectra (XPS) were carried out on an Escalab250Xi photoelectron spectrometer (Thermo Fisher Scientific). The photothermal properties were measured with a NIR laser (Hi-Tech Optoelectronics Co. Ltd., China).

Preparation of PDA/Cu Nanometer Rods. PDA/Cu nanometer rods were prepared as previously described with modifications.[31] In a typical procedure, an aqueous solution of $CuSO_4·5H_2O$ (4 mM) and NaAc (24 mM) was kept at 55 °C with gentle stirring for 1 h to prepare the bladed $Cu_4(OH)_6SO_4$ crystals. During this time the mixture changed from a blue solution to a green suspension (at pH 5.0). Then, DA·HCl (2 g L^{-1}) was added, and the mixture was kept at 55 °C for 9 h with gentle stirring to prepare PDA/Cu nanometer rods. To analyze the kinetics of the growth of the PDA coating, the samples were collected at 0.5, 1, and 3 h after the addition of DA·HCl for further characterization. All these samples were purified by repeated centrifugation (12 000 rpm, 8 min) and dried via the freeze-drying process (−60 °C, 1 Pa, 48 h) on an LGJ-10 vacuum freeze dryer (Beijing Songyuan Huaxing Technology Develop Co. Ltd., China). Two grams per liter DA·HCl was added to the Tris−HCl buffer (0.1 M, pH 8.5) and stirred for 12 h to prepare self-polymerized PDA.

Peroxidase-Like Activity of PDA/Cu Nanometer Rods and Kinetic Assay. The peroxidase-like activity measurements were carried out in an MES aqueous buffer (pH 5.5) at 25 °C, monitoring the absorbance changes at 652 nm every 10 s over 3 min on a Hitachi U-2900 UV−vis spectrophotometer (Hitachi High-Tech, Japan) with a circulating bath. To calculate the kinetic constants, experiments were performed by determining the concentrations of H_2O_2 (100 mM), NH_4Cl (100 mM), and PDA/Cu nanometer rods (50 μg mL^{-1}) and changing the concentration of TMB (0.05−0.6 mM), or by determining the concentrations of TMB (0.5 mM), NH_4Cl (100 mM), and PDA/Cu nanometer rods (50 μg mL^{-1}) and changing the concentration of H_2O_2 (10−120 mM).

The kinetic parameters V_{max} and K_m were calculated by fitting to the Michaelis−Menten equation (eq 1)

$$v = \frac{V_{max}[S]}{K_m + [S]} \quad (1)$$

[S] is the substrate concentration, V_{max} is the maximum reaction rate, and K_m is the Michaelis constant, v is the initial reaction rate. Briefly, $v = k/\varepsilon$, k is the slope of the linear change in absorbance and ε is the molar absorption coefficient of a colorimetric substrate.

Temperature, pH, and Solution-Dependent Peroxidase-Like Activity. The effect of Cl^- concentration on catalytic activity was performed with fixed concentrations of TMB (0.5 mM), H_2O_2 (100 mM), and PDA/Cu nanometer rods (50 μg mL^{-1}).

The pH-dependent peroxidase-like catalytic activity was carried out at 25 °C in BR buffers with different pH values, and

https://doi.org/10.1021/acsomega.2c02986
ACS Omega 2022, 7, 29984−29994

the concentrations of TMB, H_2O_2, PDA/Cu nanometer rods, and NH_4Cl were 0.5 mM, 50 mM, 20 μg mL^{-1}, and 50 mM, respectively.

The temperature-dependent peroxidase-like catalytic activity of PDA/Cu nanometer rods toward OPD was measured in the BR buffer (pH 5.0), with the fixed concentrations of OPD (0.5 mM), H_2O_2 (20 mM), PDA/Cu nanometer rods (20 μg mL^{-1}), and NH_4Cl (20 mM). The parameters E_a was calculated by fitting to the Arrhenius equation (eq 2).

$$\ln k_T = -\frac{E_a}{RT} + \ln A \quad (2)$$

R, T, E_a, A, and k_T are the molar gas constant, the temperature, the activation energy, the frequency factor, and the rate constant, respectively.

Peroxidase-Like Catalytic Antimicrobial Activity. The antibacterial activity was measured against the Gram-positive bacteria *S. aureus* (*S. aureus* ATCC 25923) and the Gram-negative bacteria *E. coli* (*E. coli* DSM 4230) in the PBS buffer (pH 5.0, adjusted with 2 mol L^{-1} HCl). Briefly, a single colony was picked and cultured in 10 mL of LB medium at 37 °C. After incubating overnight in a shaking bath (shaking rate = 120 rpm), the bacterial suspension was diluted and had the final optical density of 0.5 (OD_{600nm} = 0.5), which was measured on a VICTOR X5 microplate reader (PerkinElmer, Waltham).

To find out the relationship between the antibacterial performance and the concentrations of H_2O_2 or PDA/Cu nanometer rods, the prepared bacteria suspension (50 μL) was incubated with a range of different concentrations of H_2O_2 and PDA/Cu nanometer rods for 1 h (final volume 1 mL) and studied by the plate-counting method. Furthermore, the samples after incubation were diluted tenfold and inoculated on a LB agar medium (50 μL per plate), incubated at 37 °C for 20 h, and then photographed.

The morphology of bacteria exposed to different treatments was observed by SEM. *S. aureus* and *E. coli* in the groups of the PBS buffer (pH 5.0), PDA/Cu nanometer rods, H_2O_2, and PDA/Cu nanometer rods + H_2O_2 were washed with PBS (pH 7.4), centrifuged (6000 rpm, 5 min), and resuspended in 2.5% glutaraldehyde (12 h, 4 °C). The samples were then dehydrated with a series of ethanol solutions (50−100%) and dried in air.

To identify the role of PDA/Cu nanometer rods and the released Cu^{2+} in the antibacterial process, the release of Cu^{2+} was quantified. PDA/Cu nanometer rods were suspended in pH 5.0 PBS with a concentration of 1 mg mL^{-1}, incubated at 37 °C, and the filtrate at different times (5 min, 1 h, 3 h, and 18 h) was collected. The samples of the PBS buffer (pH 5.0), $CuSO_4$ solutions (0.6 and 2 mM), PDA/Cu nanometer rods (1 mg mL^{-1}), and the filtrates were added into the probe solution (0.05 wt % dicyclohexanoneoxaly dihydrazone). All of the samples were incubated at 25 °C for 10 min and measured on a VICTOR X5 microplate reader. PDA/Cu nanometer rods incubated in the PBS buffer for 1 h were centrifuged to remove the supernatant, redispersed in water, and subjected to antibacterial experiments.

Photothermal Performance of PDA/Cu Nanometer Rods. PDA/Cu nanometer rods aqueous solutions (2 mL) at different concentrations (20−400 μg mL^{-1}) were exposed to NIR laser for 20 min (808 nm, 0.5 W cm^{-2}). The water and $Cu_4(OH)_6SO_4$ crystals (200 μg mL^{-1}) were also performed under the same conditions. In addition, the temperature changes of PDA/Cu nanometer rods (200 μg mL^{-1}) under different power densities (0.5, 1.0, and 2.0 W cm^{-2}) were recorded. The heating and cooling curve data of $Cu_4(OH)_6SO_4$ crystals (200 μg mL^{-1}) and PDA/Cu nanometer rods (200 μg mL^{-1}) were then used to calculate the photothermal conversion efficiency (η), as described by Shu et al.[35]

Photothermal and Catalytic Synergistic Antibacterial Therapy. A suspension of *S. aureus* and *E. coli* (50 μL, $OD_{600\ nm}$ = 0.5) was incubated with H_2O_2, DA/Cu nanometer rods, and H_2O_2 + PDA/Cu nanometer rods. The bacteria survival of different groups was immediately studied by the plate-counting method after being irradiated for 20 min using a NIR laser (808 nm, 40 mW cm^{-2}). The samples without laser were incubated at room temperature (25 °C) for 20 min as control groups.

■ ASSOCIATED CONTENT

Supporting Information

The Supporting Information is available free of charge at https://pubs.acs.org/doi/10.1021/acsomega.2c02986.

Characterization results, peroxidase-like activity measurements, bacteria in the PBS buffer of pH 5.0, photothermal performance, composition of the applied buffers, and the mechanism of OPD and TMB color reaction (PDF)

■ AUTHOR INFORMATION

Corresponding Authors

Thomas Maskow − *Department of Environmental Microbiology, UFZ, Helmholtz Centre for Environmental Research, 04318 Leipzig, Germany;* orcid.org/0000-0003-2939-5723; Phone: +49 341 2351328; Email: Thomas.maskow@ufz.de

Yi Liu − *Department of Chemistry, College of Chemistry and Molecular Sciences, Wuhan University, Wuhan 430072, P. R. China; State Key Laboratory of Membrane Separation and Membrane Process & Tianjin Key Laboratory of Green Chemical Technology and Process Engineering, School of Chemistry, Tiangong University, Tianjin 300387, P. R. China;* orcid.org/0000-0001-7626-0026; Phone: +86-27-68756667; Email: yilliuchem@whu.edu.cn

Authors

Lian-Jiao Zhou − *Department of Chemistry, College of Chemistry and Molecular Sciences, Wuhan University, Wuhan 430072, P. R. China*

Yu-Ying Wang − *Department of Chemistry, College of Chemistry and Molecular Sciences, Wuhan University, Wuhan 430072, P. R. China*

Shu-Lan Li − *Department of Chemistry, College of Chemistry and Molecular Sciences, Wuhan University, Wuhan 430072, P. R. China; State Key Laboratory of Membrane Separation and Membrane Process & Tianjin Key Laboratory of Green Chemical Technology and Process Engineering, School of Chemistry, Tiangong University, Tianjin 300387, P. R. China;* orcid.org/0000-0001-8537-8763

Ling Cao − *Department of Chemistry, College of Chemistry and Molecular Sciences, Wuhan University, Wuhan 430072, P. R. China*

Feng-Lei Jiang − *Department of Chemistry, College of Chemistry and Molecular Sciences, Wuhan University,*

https://doi.org/10.1021/acsomega.2c02986
ACS Omega 2022, 7, 29984−29994

Wuhan 430072, P. R. China; orcid.org/0000-0002-1008-6042

Complete contact information is available at: https://pubs.acs.org/10.1021/acsomega.2c02986

Notes

The authors declare no competing financial interest.

■ ACKNOWLEDGMENTS

The authors gratefully acknowledge financial support from the National Key R&D Program of China (2018YFA0703700) and the National Natural Science Foundation of China (No. 22073070).

■ REFERENCES

(1) Gupta, A.; Mumtaz, S.; Li, C. H.; Hussain, I.; Rotello, V. M. Combatting Antibiotic-Resistant Bacteria Using Nanomaterials. *Chem. Soc. Rev.* **2019**, *48*, 415−427.

(2) Pelgrift, R. Y.; Friedman, A. J. Nanotechnology as A Therapeutic Tool to Combat Microbial Resistance. *Adv. Drug Delivery Rev.* **2013**, *65*, 1803−1815.

(3) Rashki, S.; Asgarpour, K.; Tarrahimofrad, H.; Hashemipour, M.; Ebrahimi, M. S.; Fathizadeh, H.; Khorshidi, A.; Khan, H.; Marzhoseyni, Z.; Salavati-Niasari, M.; Mirzaei, H. Chitosan-Based Nanoparticles against Bacterial Infections. *Carbohydr. Polym.* **2021**, *251*, No. 117108.

(4) Wang, C. Y.; Makvandi, P.; Zare, E. N.; Tay, F. R.; Niu, L. N. Advances in Antimicrobial Organic and Inorganic Nanocompounds in Biomedicine. *Adv. Ther.* **2020**, *3*, No. 2000024.

(5) Yoon, K. Y.; Byeon, J. H.; Park, J. H.; Hwang, J. Susceptibility Constants of *Escherichia coli* and *Bacillus subtilis* to Silver and Copper Nanoparticles. *Sci. Total Environ.* **2007**, *373*, 572−575.

(6) Xi, J. Q.; Wei, G.; An, L. F.; Xu, Z. B.; Xu, Z. L.; Fan, L.; Gao, L. Z. Copper/Carbon Hybrid Nanozyme: Tuning Catalytic Activity by the Copper State for Antibacterial Therapy. *Nano Lett.* **2019**, *19*, 7645−7654.

(7) Hu, L. Z.; Yuan, Y. L.; Zhang, L.; Zhao, J. M.; Majeed, S.; Xu, G. B. Copper Nanoclusters as Peroxidase Mimetics and Their Applications to H_2O_2 and Glucose Detection. *Anal. Chim. Acta* **2013**, *762*, 83−86.

(8) Wu, J. J. X.; Wang, X. Y.; Wang, Q.; Lou, Z. P.; Li, S. R.; Zhu, Y. Y.; Qin, L.; Wei, H. Nanomaterials with Enzyme-Like Characteristics (Nanozymes): Next-Generation Artificial Enzymes (II). *Chem. Soc. Rev.* **2019**, *48*, 1004−1076.

(9) Liu, Q. W.; Zhang, A.; Wang, R. H.; Zhang, Q.; Cui, D. X. A Review on Metal- and Metal Oxide-Based Nanozymes: Properties, Mechanisms, and Applications. *Nano-Micro Lett.* **2021**, *13*, No. 154.

(10) Bokare, A. D.; Choi, W. Review of Iron-Free Fenton-Like Systems for Activating H_2O_2 in Advanced Oxidation Processes. *J. Hazard. Mater.* **2014**, *275*, 121−135.

(11) Voinov, M. A.; Pagan, J. O. S.; Morrison, E.; Smirnova, T. I.; Smirnov, A. I. Surface-Mediated Production of Hydroxyl Radicals as a Mechanism of Iron Oxide Nanoparticle Biotoxicity. *J. Am. Chem. Soc.* **2011**, *133*, 35−41.

(12) Li, Y. Y.; Zhu, W. X.; Li, J. S.; Chu, H. T. Research Progress in Nanozyme-Based Composite Materials for Fighting Against Bacteria and Biofilms. *Colloid Surf., B* **2021**, *198*, No. 111465.

(13) Vatansever, F.; de Melo, W.; Avci, P.; Vecchio, D.; Sadasivam, M.; Gupta, A.; Chandran, R.; Karimi, M.; Parizotto, N. A.; Yin, R.; Tegos, G. P.; Hamblin, M. R. Antimicrobial Strategies Centered Around Reactive Oxygen Species - Bactericidal Antibiotics, Photodynamic Therapy, and Beyond. *FEMS Microbiol. Rev.* **2013**, *37*, 955−989.

(14) Karim, M. N.; Singh, M.; Weerathung, P.; Bian, P.; Zheng, R.; Dekiwadia, C.; Ahmed, T.; Walia, S.; Della Gaspera, E.; Singh, S.; Ramanathan, R.; Bansal, V. Visible-Light-Triggered Reactive-Oxygen-Species-Mediated Antibacterial Activity of Peroxidase-Mimic CuO Nanorods. *ACS Appl. Nano Mater.* **2018**, *1*, 1694−1704.

(15) Wang, X. W.; Shi, Q. Q.; Zha, Z. B.; Zhu, D. D.; Zheng, L. R.; Shi, L. X.; Wei, X. W.; Lian, L.; Wu, K. L.; Cheng, L. Copper Single-Atom Catalysts with Photothermal Performance and Enhanced Nanozyme Activity for Bacteria-Infected Wound Therapy. *Bioact. Mater.* **2021**, *6*, 4389−4401.

(16) Liu, Y. F.; Nie, N.; Tang, H. F.; Zhang, C. R.; Chen, K. Z.; Wang, W.; Liu, J. F. Effective Antibacterial Activity of Degradable Copper-Doped Phosphate-Based Glass Nanozymes. *ACS Appl. Mater. Interfaces* **2021**, *13*, 11631−11645.

(17) Fu, Y.; Yang, L.; Zhang, J. H.; Hu, J. F.; Duan, G. G.; Liu, X. H.; Li, Y. W.; Gu, Z. P. Polydopamine Antibacterial Materials. *Mater. Horiz.* **2021**, *8*, 1618−1633.

(18) He, S. Y.; Feng, Y.; Sun, Q.; Xu, Z. A.; Zhang, W. Charge-Switchable CuxO Nanozyme with Peroxidase and Near-Infrared Light Enhanced Photothermal Activity for Wound Antibacterial Application. *ACS Appl. Mater. Interfaces* **2022**, *14*, 25042−25049.

(19) Xiao, J. Y.; Hai, L.; Li, Y. Y.; Li, H.; Gong, M. H.; Wang, Z. F.; Tang, Z. F.; Deng, L.; He, D. G. An Ultrasmall Fe_3O_4-Decorated Polydopamine Hybrid Nanozyme Enables Continuous Conversion of Oxygen into Toxic Hydroxyl Radical via GSH-Depleted Cascade Redox Reactions for Intensive Wound Disinfection. *Small* **2022**, *18*, No. 2105465.

(20) Li, Y.; Fu, R. Z.; Duan, Z. G.; Zhu, C. H.; Fan, D. D. Mussel-Inspired Adhesive Bilayer Hydrogels for Bacteria-Infected Wound Healing via NIR-Enhanced Nanozyme Therapy. *Colloid Surf., B* **2022**, *210*, No. 112230.

(21) Moon, H.; Lee, Y. C.; Hur, J. One-Pot Decoration of Cupric Oxide on Activated Carbon Fibers Mediated by Polydopamine for Bacterial Growth Inhibition. *Materials* **2020**, *13*, No. 1158.

(22) Zittlau, A. H.; Shi, Q.; Boerio-Goates, J.; Woodfield, B. F.; Majzlan, J. Thermodynamics of the Basic Copper Sulfates Antlerite, Posnjakite, and Brochantite. *Geochemistry* **2013**, *73*, 39−50.

(23) Salomäki, M.; Ouvinen, T.; Marttila, L.; Kivela, H.; Leiro, J.; Makila, E.; Lukkari, J. Polydopamine Nanoparticles Prepared Using Redox-Active Transition Metals. *J. Phys. Chem. B* **2019**, *123*, 2513−2524.

(24) Tu, Y. X.; Lei, C. F.; Deng, F.; Chen, Y.; Wang, Y.; Zhang, Z. K. Core-Shell ZIF-8@Polydopamine Nanoparticles Obtained by Mitigating the Polydopamine Coating Induced Self-Etching of MOFs: Prototypical Metal Ion Reservoirs for Sticking to and Killing Bacteria. *New J. Chem.* **2021**, *45*, 8701−8713.

(25) Pham, A. N.; Waite, T. D. Cu(II)-Catalyzed Oxidation of Dopamine in Aqueous Solutions: Mechanism and Kinetics. *J. Inorg. Biochem.* **2014**, *137*, 74−84.

(26) Salomäki, M.; Marttila, L.; Kivela, H.; Ouvinen, T.; Lukkari, J. Effects of pH and Oxidants on the First Steps of Polydopamine Formation: A Thermodynamic Approach. *J. Phys. Chem. B* **2018**, *122*, 6314−6327.

(27) Massaro, M.; Armetta, F.; Cavallaro, G.; Martino, D. F. C.; Gruttadauria, M.; Lazzara, G.; Riela, S.; d'Ischia, M. Effect of Halloysite Nanotubes Filler on Polydopamine Properties. *J. Colloid Interface Sci.* **2019**, *555*, 394−402.

(28) Gürbüz, M. U.; Elmaci, G.; Erturk, A. S. In Situ Deposition of Silver Nanoparticles on Polydopamine-Coated Manganese Ferrite Nanoparticles: Synthesis, Characterization, and Application to the Degradation of Organic Dye Pollutants as an Efficient Magnetically Recyclable Nanocatalyst. *Appl. Organomet. Chem.* **2021**, *35*, No. e6284.

(29) Shen, H.; Guo, J.; Wang, H.; Zhao, N.; Xu, J. Bioinspired Modification of h-BN for High Thermal Conductive Composite Films with Aligned Structure. *ACS Appl. Mater. Interfaces* **2015**, *7*, 5701−5708.

(30) Perez-Benito, J. F. Copper(II)-Catalyzed Decomposition of Hydrogen Peroxide: Catalyst Activation by Halide Ions. *Monatsh. Chem.* **2001**, *132*, 1477−1492.

(31) Gao, L. Z.; Zhuang, J.; Nie, L.; Zhang, J. B.; Zhang, Y.; Gu, N.; Wang, T. H.; Feng, J.; Yang, D. L.; Perrett, S.; Yan, X. Intrinsic

Peroxidase-Like Activity of Ferromagnetic Nanoparticles. *Nat. Nanotechnol.* **2007**, *2*, 577−583.
(32) Zheng, H. Q.; Liu, C. Y.; Zeng, X. Y.; Chen, J.; Lu, J.; Lin, R. G.; Cao, R.; Lin, Z. J.; Su, J. W. MOF-808: A Metal-Organic Framework with Intrinsic Peroxidase-Like Catalytic Activity at Neutral pH for Colorimetric Biosensing. *Inorg. Chem.* **2018**, *57*, 9096−9104.
(33) Wang, Y. H.; Yao, J. C.; Cao, Z. L.; Fu, P.; Deng, C.; Yan, S. F.; Shi, S.; Zheng, J. P. Peroxidase-Mimetic Copper-Doped Carbon-Dots for Oxidative Stress-Mediated Broad-Spectrum and Efficient Antibacterial Activity. *Chem.—Eur. J.* **2022**, *28*, No. e202104174.
(34) Lin, T. R.; Zhong, L. S.; Guo, L. Q.; Fu, F. F.; Chen, G. N. Seeing Diabetes: Visual Detection of Glucose Based on the Intrinsic Peroxidase-Like Activity of MoS_2 Nanosheets. *Nanoscale* **2014**, *6*, 11856−11862.
(35) Shu, Q. F.; Liu, J.; Chang, Q.; Liu, C. H.; Wang, H. F.; Xie, Y. J.; Deng, X. Y. Enhanced Photothermal Performance by Carbon Dot-Chelated Polydopamine Nanoparticles. *ACS Biomater. Sci. Eng.* **2021**, *7*, 5497−5505.
(36) Fan, S. N.; Jiang, X. X.; Yang, M. H.; Wang, X. G. Sensitive Colorimetric Assay for the Determination of Alkaline Phosphatase Activity Utilizing Nanozyme Based on Copper Nanoparticle-Modified Prussian Blue. *Anal. Bioanal. Chem.* **2021**, *413*, 3955−3963.
(37) Wang, L.; Hou, J. J.; Li, S. Z.; Carrier, A. J.; Guo, T.; Liang, Q. S.; Oakley, D.; Zhang, X. Cuo Nanoparticles as Haloperoxidase-Mimics: Chloride-Accelerated Heterogeneous Cu-Fenton Chemistry for H_2O_2 And Glucose Sensing. *Sens. Actuator, B* **2019**, *287*, 180−184.
(38) Linzner, N.; Van Loi, V.; Fritsch, V. N.; Antelmann, H. Thiol-Based Redox Switches in the Major Pathogen *Staphylococcus aureus*. *Biol. Chem.* **2021**, *402*, 333−361.
(39) Wang, H. X.; Liao, B.; Hu, M. Y.; Ai, Y. L.; Wen, L. J.; Yang, S.; Ye, Z.; Qin, J.; Liu, G. Heterogeneous Activation of Peroxymonosulfate by Natural Chalcopyrite for Efficient Remediation of Groundwater Polluted by Aged Landfill Leachate. *Appl. Catal., B* **2022**, *300*, No. 120744.
(40) Liu, Y. L.; Ai, K. L.; Lu, L. H. Polydopamine and Its Derivative Materials: Synthesis and Promising Applications in Energy, Environmental, and Biomedical Fields. *Chem. Rev.* **2014**, *114*, 5057−5115.
(41) Salomäki, M.; Tupala, M.; Parviainen, T.; Leiro, J.; Karonen, M.; Lukkari, J. Preparation of Thin Melanin-Type Films by Surface-Controlled Oxidation. *Langmuir* **2016**, *32*, 4103−4112.

https://doi.org/10.1021/acsomega.2c02986
ACS Omega 2022, 7, 29984−29994